I&EC research
Industrial & Engineering Chemistry Research

pubs.acs.org/IECR

Article

Phosphonated Lower-Molecular-Weight Polyethyleneimines as Oilfield Scale Inhibitors: An Experimental and Theoretical Study

Mohamed F. Mady,* Ali H. Karaly, Safwat Abdel-Azeim, Ibnelwaleed A. Hussein, Malcolm A. Kelland, and Ahmed Younis

Cite This: *Ind. Eng. Chem. Res.* 2022, 61, 9586−9599

Read Online

ACCESS | Metrics & More | Article Recommendations | Supporting Information

ABSTRACT: For many years, amino methylenephosphonate ($-CH_2-N-PO_3H_2$)-based scale inhibitors (SIs) have been deployed for preventing various scales in the oil and gas industry, particularly for squeeze treatment applications. However, this class of phosphonate inhibitors showed several limitations related to environmental concerns and compatibility with brine solutions. The low toxicity of low-molecular-weight polyethyleneimine (LMW-PEI) encouraged us to phosphonate a series of branched and linear PEIs via the Moedritzer−Irani reaction. The phosphonated polyethyleneimine PPEIs are branched PPEI-600, branched PPEI-1200, branched PPEI-2000, and linear PPEI-5000. The newly synthesized PPEIs (branched and linear) were screened for calcium carbonate and barium sulfate utilizing a high-pressure dynamic tube-blocking rig at 100 °C and 80 bar. Moreover, we report the compatibility activity of all PPEIs with various concentrations of calcium ions (up to 10000 ppm). The morphology of the calcium carbonate and barium sulfate scale crystals in the absence and presence of linear PPEI-5000 was also investigated under static conditions using scanning electron microscopy (SEM). The obtained results showed that all branched and linear PPEIs gave moderate calcite and barite inhibition activities. It was also found that all branched PPEIs gave moderate to poor calcium compatibility at high dosages of calcium ions (1000−10 000 ppm). Interestingly, linear PPEI-5000 displayed superior compatibility properties at high dosages of SI (up to 50 000 ppm) and high concentrations of Ca^{2+} ions (up to 10 000 ppm). Furthermore, field emission scanning electron microscopy analysis confirmed that the crystal shapes of $CaCO_3$ and $BaSO_4$ mineral scales are greatly changed in the presence of linear PPEI-5000. At high dosages of linear PPEI-5000 SI (100 ppm), the $CaCO_3$ crystals are completely converted from cubic-shaped blocks (blank calcite) into long cluster shapes. Density functional theory (DFT) simulations reveal favorable interactions of PPEI polymers with the two mineral facets (calcite and barite) with more affinity toward the calcite surface. PPEI with more phosphonate groups exhibits affinities comparable to the commercial-scale inhibitors. The high density of the phosphonate groups on the branched PPEI and its strong affinity toward calcium ions explain its poor calcium compatibility. The polymer flocculation and sluggish barite kinetics are the potential reasons for its low performance against the barite scale.

1. INTRODUCTION

Flow assurance management in the upstream oil and gas industry aims to ensure continuity of hydrocarbon production without interruption. Gas hydrates, corrosion, and inorganic scales are the commonest flow assurance problems in oilfield installations.[1] Scaling is considered one of the major issues during the production of well fluids. Oilfield scaling is the deposition of sparingly soluble inorganic salts from aqueous supersaturated solutions.[1,2] These mineral scales are generally formed in the petroleum reservoir due to chemical intolerance between well brines (formation water) and injection water (seawater).[3,4] The oilfield scale can adhere to any surface. If there is no quick treatment for the scale deposition, the surface layer will continue to become thicker. This will lead to blocking the pore throats and loss in hydrocarbon production.[3,5]

Commonly encountered scales in the upstream oil and gas industry are calcium carbonate ($CaCO_3$, calcite), sulfates of Group II, such as barium sulfate ($BaSO_4$, barite), calcium sulfate ($CaSO_4·2H_2O$, gypsum), and strontium sulfate ($SrSO_4$, celestite).[6,7] Calcium carbonate minerals are temperature- and pressure-dependent scales.[8] Calcite fouling is caused due to the equilibrium between bicarbonate, carbonate, and carbon dioxide in the well reservoir. On the contrary, sulfate scales are formed when the metal ions (e.g., calcium, magnesium, and

Received: May 16, 2022
Revised: June 15, 2022
Accepted: June 24, 2022
Published: July 5, 2022

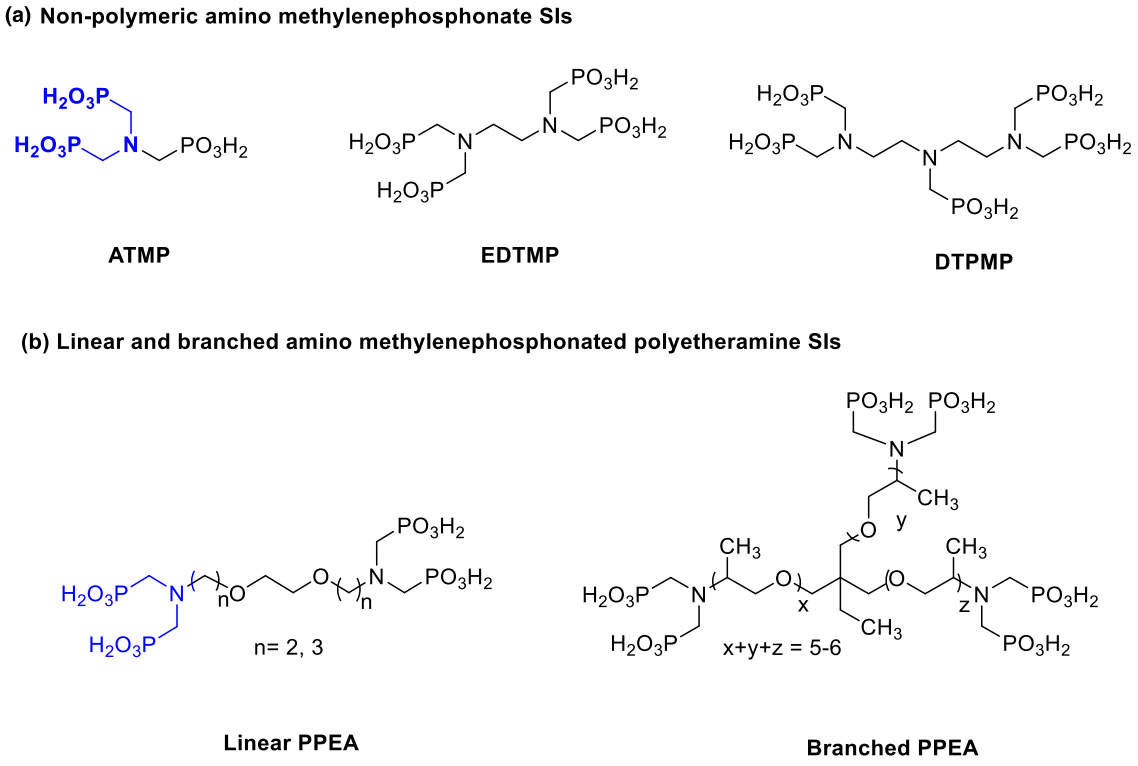

Figure 1. Chemical structures of amino methylenephosphonate-based scale inhibitors. (a) Commercial SIs (A: ATMP, EDTMP, and DTPMP) and (b) linear and branched amino methylenephosphonated polyetheramines developed by our group.

barium) interact with sulfate ions. This sulfate fouling is not an essential function of the well brines' pH (pH-independent).[9,10]

Many techniques have been utilized to mitigate the deposition of inorganic scales in the petroleum industry.[4,11] Chemical treatment approaches, particularly scale inhibition, play a vital role in preventing and mitigating scale fouling in the topside and downhole oilfield applications.[12] Low-dosage water-soluble scale inhibitors (SIs) are widely deployed as a cost-effective treatment for controlling scale formation. SIs prevent nucleation, crystal growth, and deposition of inorganic salts in petroleum reservoirs.[1,13,14]

For many years, amino methylenephosphonate-based SIs ($-CH_2-N-PO_3H_2$) have been deployed for preventing various scales in the oil and gas industry.[15] Several commercial amino methylenephosphonate SIs are available in the market, providing excellent inhibition performance, particularly for squeeze treatment applications,[16,17] for example, aminotris methylenephosphonic acid (ATMP), diethylenetriamine pentamethylene phosphonic acid (DTPMP), and ethylenediamine tetramethylene phosphonic acid (EDTMP).[1] The chemical structures of these commercial SIs are shown in Figure 1. However, this class of phosphonate inhibitors showed several limitations related to environmental concerns (as outlined by the Oslo and Paris (OSPAR) Commission) and compatibility with the brine solutions.[18,19] Therefore, our Green and Sustainable Oilfield Chemistry Group at the University of Stavanger has made several attempts to develop environmentally acceptable SIs incorporating a $-CH_2-N-PO_3H_2$ moiety.[20−22] For example, we have recently synthesized a series of linear and branched phosphonated polyetheramines (PPEAs) as environmentally friendly SIs for calcite and barite scales according to the Heidrun oilfield, North Sea, Norway (Figure 1).[23] The results showed that linear PPEAs displayed excellent inhibition performance against calcite and barite scales using a high-pressure dynamic tube-blocking rig at 80 bar and 100 °C. Moreover, linear PPEAs exhibited superior tolerance with high Ca^{2+} ions (up to 10 000 ppm) and very good thermal stability and biodegradation properties.

Polyethyleneimine (PEI) is an amino-rich hydrophilic cationic polymer, containing several primary, secondary, and tertiary amine groups in its structural backbone.[24,25] PEI has been attracting great attention due to its widespread industrial and medical applications in recent decades.[26,27] It is well known that PEI is widely used as a nonviral gene delivery carrier.[28] In addition, this class of cationic polymers showed outstanding metal-binding activities.[29,30] For example, modified polyethyleneimine with phosphonate groups (PPEI) was used as a chelating agent for rare earth elements.[31−35] Furthermore, Demadis et al. reported that PPEIs showed a good inhibition efficiency against silica scales.[36−38]

Indeed, PEI and its derivatives showed a wide range of various industrial applications, such as anticorrosion, agricultural, water, and wastewater treatment applications.[34] The chemical structure of PEI can be presented in two forms, which are branched and linear, incorporating amine groups in the structure chain.[39,40] Linear PEI has been prepared in two steps: (1) cationic ring-opening polymerization of an oxazoline moiety and (2) acidic or basic hydrolysis of linear polyoxazoline to afford linear PEI. In addition, branched PEI has been synthesized by acid-catalyzed cationic ring-opening of aziridine.[39,40] Figure 2 shows the synthesis routes of linear and branched PEIs. It was reported that the molecular weight of PEI plays an important role in determining its toxicity. Low-molecular-weight polyethyleneimine (LMW-PEI) improved the cytotoxicity and biodegradation properties compared to high-molecular-weight polyethyleneimine (HMW-PEI).[41−45]

In this project, the low toxicity of LMW-PPEI motivated us to phosphonate a series of branched and linear PPEIs via the

https://doi.org/10.1021/acs.iecr.2c01730
Ind. Eng. Chem. Res. 2022, 61, 9586−9599

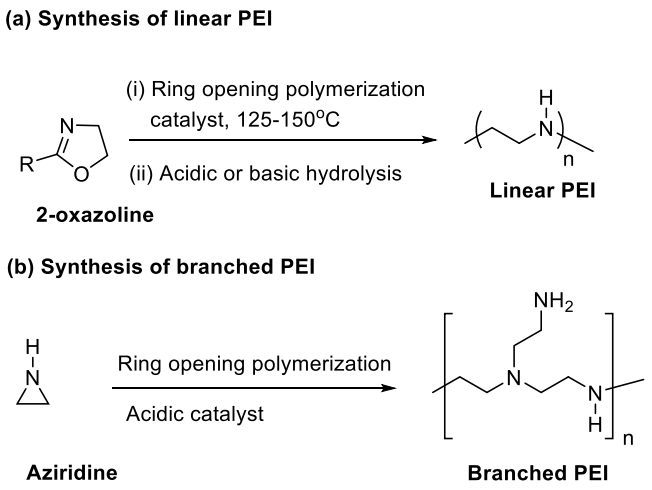

Figure 2. Synthesis route of linear and branched PEIs.

Moedritzer−Irani reaction. Three different molecular weights of branched PEIs (M_w = 600, 1200, and 2000) and one linear PEI of M_w 5000 were reacted with phosphorous acid (H_3PO_3) and formaldehyde (HCHO) in the presence of aqueous hydrochloric acid (HCl) under reflux to afford phosphonated polyethyleneimine PPEIs (branched PPEI-600, branched PPEI-1200, branched PPEI-2000, and linear PPEI-5000, respectively). All of the newly synthesized PPEIs (branched and linear) were screened for calcium carbonate (calcite) and barium sulfate (barite) utilizing a high-pressure dynamic tube-blocking rig. Moreover, we report the compatibility activity of all PPEIs with various concentrations of calcium ions (up to 10 000 ppm). We have also studied the morphology of the inorganic scale crystal in the absence and presence of SI using scanning electron microscopy (SEM) to understand the scale inhibition mechanism and compare the difference in surface morphology and crystal microstructure. In addition, quantum chemical simulations for branched and linear PPEIs were conducted to understand the scale prevention mechanism.

2. EXPERIMENTAL SECTION

2.1. Materials and Characterization. Branched polyethyleneimines PEI (M_w = 1200 and 2000) were purchased from Sigma-Aldrich (Merck) and branched PEI (M_w = 600) was purchased from Thermo Scientific. Linear polyethyleneimine PEI (M_w = 5000) was obtained from Sigma-Aldrich (Merck). All other chemicals and solvents were received from VWR, Nippon Chemical Industrial Co., Ltd., and Tokyo Chemical Industry Co., Ltd. and utilized as received without further purification. Deionized water with a conductivity of 18 MΩ was obtained from ELGA PURELAB Prima, Germany. Two commercial oilfield SIs diethylenetriamine pentakis-(methylenephosphonic acid) (DTPMP) and aminotris-(methylenephosphonic acid) (ATMP) were supplied by Italmatch Chemicals S.p.A., Italy.

The chemical structures of all synthesized PPEI-based SIs were characterized and elucidated by ^{1}H and ^{31}P nuclear magnetic resonance (NMR) spectroscopy. ^{1}H and ^{31}P NMR experiments were performed at 25 °C using a 400 MHz Bruker NMR spectrometer in the presence of deuterium oxide (D_2O) as a solvent. The pH of all NMR samples was adjusted in the range of 2−3. Moreover, the ^{31}P NMR spectra were not ^{1}H coupled. ^{1}H and ^{31}P NMR chemical shifts (δ) of all target products were obtained in D_2O.

2.2. Preparation of Branched and Linear Polyethyleneimine (PPEI)-Based Oilfield Scale Inhibitors. A general procedure for the preparation of branched phosphonated

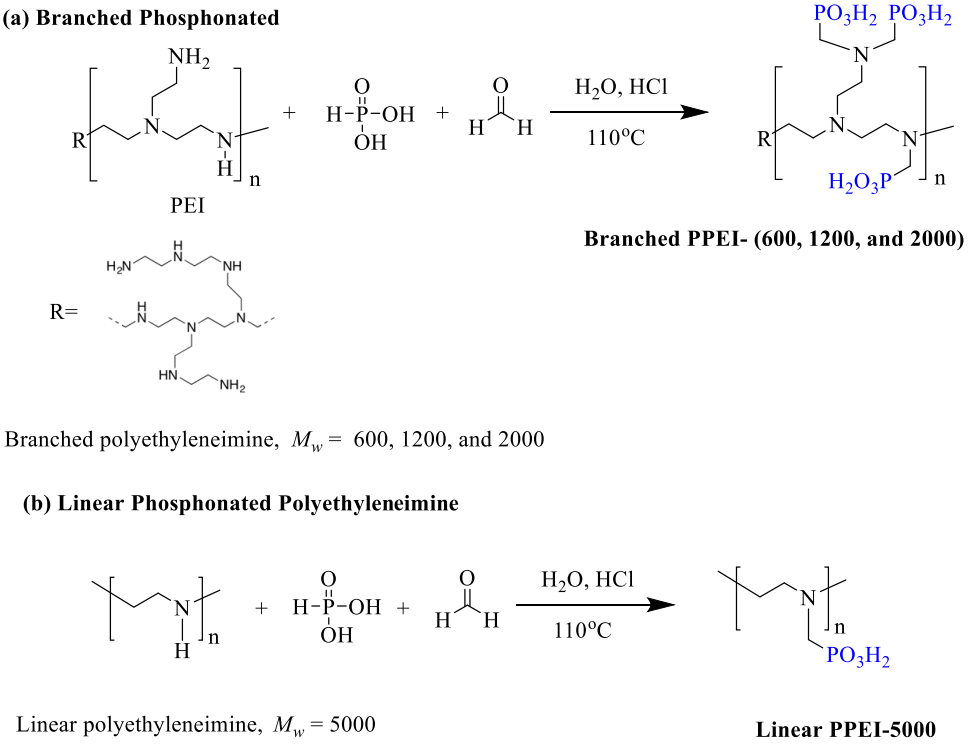

Figure 3. Synthesis of phosphonated polyethyleneimines via the Moedritzer−Irani reaction: (a) branched phosphonated polyethyleneimines (M_w = 600, 1200, and 2000) and (b) linear phosphonated polyethyleneimine (M_w = 5000).

https://doi.org/10.1021/acs.iecr.2c01730
Ind. Eng. Chem. Res. 2022, 61, 9586−9599

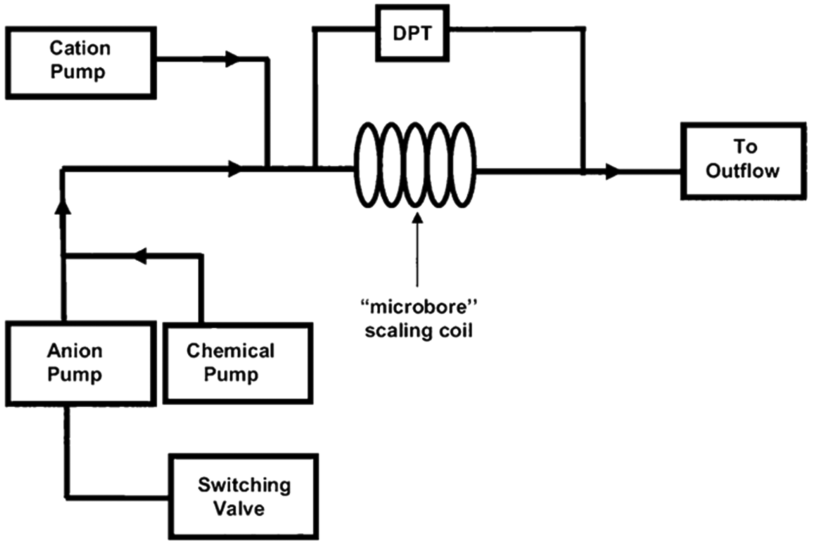

Figure 4. Schematic diagram of the dynamic scale rig for scale inhibitor testing.

polyethyleneimine (branched PPEI) and linear phosphonated polyethyleneimine (linear PPEI) using the Moedritzer−Irani reaction is discussed below.

A series of branched polyethyleneimines with different molecular weights (M_w = 600, 1200, and 2000), and one linear polyethyleneimine (molecular mass = 5000) were phosphonated by treating PEI with formaldehyde and phosphorous acid in the presence of hydrochloric acid, as described by Moedritzer et al.[46] Figure 3 presented the general synthesis pathway of linear and branched PPEIs.

A typical procedure for the synthesis of linear PPEI is as follows: linear polyethyleneimine (M_w = 5000) (1.5 g, ca. 34.8 mmol equivalents of aziridine monomer units) was added to a 150 mL two-neck round bottom flask connected with a reflux condenser, a magnetic stirrer, and a thermometer. Phosphorous acid (H_3PO_3, 2.86 g, 34.8 mmol) was dissolved in distilled water (10 mL, Milli-Q water) and then added dropwise to the round bottom flask, followed by the addition of HCl 37% (3.43 g, 34.8 mmol). The resulting solution was warmed to 60 °C under nitrogen gas. Then, aqueous formaldehyde 37% (HCHO, 2.83 g, 34.8 mmol) was added slowly over the course of 1 h. The temperature of the mixture was increased to 110 °C and refluxed under vigorous stirring for 72 h. The reaction mixture was then cooled to room temperature. The liquid phases of the reaction mixture were mixed with diethyl ether (2 × 25 mL) and shaken well. The washing solvent of diethyl ether was separated using a separating funnel to leave the aqueous solution of PPEIs. The water phase of the mixture reaction was then removed in vacuo, giving a phosphonated linear polyethyleneimine (linear PPEI-5000) as a pale yellow oil (2.1 g). ^{31}P NMR (D_2O, 162.00 MHz): δ 19.78 ppm. For the synthesized branched PPEIs via the Moedritzer−Irani reaction, the percentage of all reactants (H_3PO_3, HCHO, and HCl) to aziridine monomer units was 3:1. All synthesized branched and linear PPEIs were characterized and elucidated by ^{1}H and ^{31}P NMR.

2.3. High-Pressure Dynamic Tube-Blocking Test Methods. The in-house high-pressure dynamic loop test has been explained many times in our published articles previously.[20−22] This procedure is an efficient laboratory method that detects the inhibition efficiency of SIs against various inorganic scales in a range of industrial applications, particularly for the oil and gas industry and water treatment. Our dynamic tube-blocking scale rig was manufactured by Scaled Solutions Ltd. (U.K.). Figure 4 shows a schematic diagram of the dynamic scale rig consisting of three pumps. Each pump supplies fluid up to 10.00 mL/min via a 316 stainless steel coil with a diameter of 1 mm and a length of 3.00 m. The stainless steel coil is placed inside an oven. To simulate the petroleum reservoir conditions, we performed all scale inhibition tests at 100 °C and approximately 80 bar.[12−18]

The main operation description of the three pumps is stated as follows: pump 1 injects Heidrun formation water (FW) cations (brine 1) with a constant flow rate of 5.00 mL/min; pump 2 injects Heidrun seawater (SW) anions (brine 2). Pump 2 was also utilized to inject the cleaning out mixture solutions. This mixture consists of a high alkaline solution of tetrasodium ethylenediaminetetraacetate (Na_4EDTA 5 wt %, pH = 11−13) in Milli-Q water. Pump 3 injects different programmed SI dosages. A 1000 ppm stock solution of the tested SI is always prepared in 500 mL of Milli-Q water. In addition, we generally adjusted the pH of all tested SIs in the range of 4−6 to simulate the oil reservoir conditions according to the Heidrun oilfield. Table S4 tabulates the exact pH for each SI test. The compositions of FW and SW in this project are synthetically prepared according to the Heidrun oilfield, Norway (Table 1). The volume mixture of SW and FW is 50:50 to afford the barium sulfate oilfield scale, except for

Table 1. Synthetic Scaling Brines (FW:SW) of the Heidrun Oilfield, Norway

ion	component	Heidrun formation water (ppm)	seawater (ppm)	50:50 mixed brine (ppm)
Na^+	NaCl	19 500	10 900	15 200
Ca^{2+}	$CaCl_2{\cdot}2H_2O$	1020	428	724
Mg^{2+}	$MgCl_2{\cdot}6H_2O$	265	1368	816
K^+	KCl	545	460	502
Ba^{2+}	$BaCl_2{\cdot}2H_2O$	285	0	142
Sr^{2+}	$SrCl_2{\cdot}6H_2O$	145	0	72
SO_4^{2-}	Na_2SO_4 anhydrous	0	2960	1480
HCO_3^-	$NaHCO_3$	880	120	500

https://doi.org/10.1021/acs.iecr.2c01730
Ind. Eng. Chem. Res. 2022, 61, 9586−9599

bicarbonate (HCO_3^-) ions. The water composition of the separate brines 1 and 2 for calcium carbonate and barium sulfate scales are presented in Tables S5 and S6, respectively. All mixture solutions (brine 1, brine 2, and cleaning fluid) were freshly prepared and degassed using a water vacuum pump for each experiment.

The high-pressure dynamic tube-blocking test results displayed the minimum inhibitor concentration (MIC) and fail inhibitor concentration (FIC). The FIC shows that the SI loses its inhibition efficiency to mitigate the deposition of inorganic salts. In contrast, the MIC refers to the tested SI that prevented the scale mineral deposition. For evaluating new SIs in the scale rig, we always programmed various SI concentrations, starting from 100 ppm and going to 50, 20, 10, 5, 2, and finally, 1 ppm throughout the test period (1 h), or until inorganic scales were formed in the stainless steel coil.

The obtained results from the dynamic tube-blocking experiments of the tested inhibitors were transferred to an Excel file. These results were converted to a schematic graph of the scaling time in minutes versus differential pressure (psi) throughout the stainless steel coil. This schematic diagram presents four stages for each experiment: the first blank test, the first scale test, the second scale test, and finally, a new second blank test.

2.4. Calcium Compatibility Test. This test aims to detect the compatibility of all newly synthesized SIs with calcium ions at different concentrations. Many commercial phosphonate-based SIs are incompatible with Ca^{2+} ions, giving SI-Ca^{2+} complex precipitation. This problem can cause formation damage and poor retention of SI onto the formation rock in the petroleum reservoir. We have screened the tolerance properties of all synthesized branched and linear PPEIs (100−50 000 ppm) at a range of Ca^{2+} dosages (up to 10 000 ppm) to check the performance of PPEIs when mixing with FW medium.

To carry out the tolerance test: several dosages of PPEIs (branched and linear) of 100, 1000, 10 000, and 50 000 ppm were added to 10 mL of deionized water in 15 mL glass vessels. In the next step, different dosages of calcium ions (100, 1000, and 10 000 ppm) were dissolved with synthetic SW (3.00% of NaCl) in the same vessels. The final pH of the resulting solution was generally adjusted at 4−6 to match the oil well pH. All bottles were shaken well, and the appearance of the solution was detected at room temperature. The vessels were then placed in the oven at 80 °C for 24 h. The tolerance properties (clear, hazy, and precipitate) of linear and branched PPEIs with Ca^{2+} were investigated by our visual observation after 30 min, 1, 4, and 24 h.

2.5. Characterization of Scale Crystals. The morphology of the mineral crystals before and after treatment under static conditions was determined using scanning electron microscopy (SEM) to understand the scale inhibition mechanism and compare the difference in surface morphology and crystal microstructure. SEM images of calcite and barite crystals were recorded using a SIGMA field emission scanning electron microscope, Zeiss Supra 35VP. To prepare the scale crystal samples for SEM analysis, the NACE Standard jar test protocol (TM0374-2007) was conducted based on the Heidrun oilfield, Norwegian Sea, Norway (Table 1), as illustrated in detail previously.[47,48] Briefly, a total volume of 40 mL of 50:50 solution of cationic brine and anionic brine are mixed and shaken well and then poured into 50 mL Schott Duran glass bottles. For the blank test (neat crystals), no SI was added to the brine solutions. For comparison, we decided to study the surface morphology of the calcium carbonate and barium sulfate scales in the presence of the superior calcium tolerance SI linear PPEI-5000 at two different concentrations. A 100 and 10 ppm of linear PPEI-5000 was mixed with the brine solutions. Then, all three bottles (blank, 100 ppm of PPEI-5000, and 10 ppm of PPEI-5000) were put in an oven at 80 °C for 5 h. The formed crystals were collected by centrifugation and washed with distilled water three times and acetone and then dried in an oven at 60 °C for 3 h. Finally, the particles were coated on SEM stubs for SEM analysis.

2.6. Quantum Chemical Calculations. *2.6.1. DFT Periodic Model Simulations.* Density functional theory (DFT) simulations were carried out using the Vienna Ab initio Simulation Package (VASP)[49,50] with the projector augmented wave pseudopotentials (PAW)[51] and the periodic boundary conditions. The Brillouin zone was sampled using 3 × 3 × 1 Monkhorst-Pack γ-centered mesh,[52] and Gaussian smearing of 0.02 eV was used for the occupation of the electronic levels. The Perdew−Burke−Ernzerhof (PBE)[53] functional within the generalized gradient approximation (GGA) was used to describe the electron interaction energy of exchange-correlation. The electronic energies were converged within the limit of 10^{-7} eV, and a cutoff of 520 eV was used. All geometries were optimized using 0.03 eV/Å force criteria. van der Waals (VDW) dispersion corrections were adopted using Grimme's D3 scheme.[54] The SIs' adsorption energies E_{ads} were calculated based on eq 1.

$$E_{ads} = E_{Slab+SI} - [E_{Slab} + E_{SI}] \quad (1)$$

For the linear PPEI, a slab of 321 supercells for the 104 calcite facet[55] and the 001 barite facet[56] are reported as the most stable facets of the calcite and barite crystals, respectively. A vacuum of 15 Å is applied along the *Z*-axis to remove the spurious interaction that could occur between the surface and its image due to the periodic boundary conditions. The thickness of the slab is composed of three layers, two layers are fixed during the geometry optimization and the top layer is allowed to relax.

2.6.2. Molecular DFT Calculations. Density functional theory calculations were carried out on one monomer of PPEI branched to calcite calcium-binding free energies. These calculations examine the calcium compatibility of PPEI polymers compared to the commercial SIs (ATMP and DTPMP) that we already reported.[57] Geometries were optimized using the wB97xd[54,58]/def2-SVP[59,60] level of theory; more accurate energies were obtained at the wB97xd/def2-TZVP level of theory. All of the stationary points were verified to be a minimum by frequency calculations and confirmed to have all positive frequencies. The solvent environment was taken into account using the PCM[61] model during the optimization of geometries. Further, we have employed the continuum solvation model based on the electronic density of the solute molecule interacting with a continuum solvent (SMD)[62] model developed by Marenich et al., which is recommended by Gaussian 16 to obtain accurate solvation free energies.[63]

Metal-binding free energies are calculated based on eq 2.

$$\Delta G_{bind} = G\text{complex} - G[\text{molecule} + \text{metal}] \quad (2)$$

The contribution of the solvation free energy to the total metal-binding free energy is calculated based on eq 3.

https://doi.org/10.1021/acs.iecr.2c01730
Ind. Eng. Chem. Res. 2022, 61, 9586−9599

$$\Delta G_{solv} = G_{solv}\ \text{complex} - G_{solv}[\text{molecule} + \text{metal}] \quad (3)$$

All binding free energies were corrected for the basis set superposition using the counterpoise method.[64,65] All calculations were performed using Gaussian 16.[63] Since, we are interested in the relative binding energies between the different SIs, the vibrational corrections to the total metal-binding free energies are neglected as they are very small compared to the vacuum binding energies and the solvation corrections (it reaches its maximum of 2 kcal/mol). Similarly, the state corrections (1.9 kcal/mol) are neglected.

3. RESULTS AND DISCUSSION

3.1. Chemistry. A series of modified LMW-PEIs (branched and linear) linked to the amino methylenephosphonate moiety (-N-CH_2-PO_3H_2) were synthesized in-house via the Moedritzer−Irani reaction. Three branched PEIs with molecular weights (M_w = 600, 1200, and 2000) and one linear PPEI (M_w = 5000) were reacted with H_3PO_3 and HCHO in a water medium as a solvent under acidic conditions (HCl) to give PPEIs, as shown in Figure 3. The obtained target chemicals are branched PPEI-600, PPEI-1200, PPEI-2000, and linear PPEI-5000. The synthesis route of PPEIs has been reported several times in the open literature under different synthetic approaches.[31,34,66,67] For example, Jensen et al. synthesized a series of amino ethylenephosphonate-hyperbranched polyethyleneimines via the Michael addition reaction in the presence of a vinyl phosphonate monomer as a phosphonating agent.[67]

The synthesized PPEIs were characterized and elucidated by ^{1}H and ^{31}P NMR spectroscopy. The chemical shifts δ (^{1}H and ^{31}P NMR) of all target products were recorded in D_2O. For example, the ^{1}H NMR spectra of branched PPEI-600 displayed a distinct doublet peak at δ 3.59−3.57 ppm that represented the -N-C**H**$_2$-PO_3H_2- moiety. It was also found that ^{1}H NMR chemical shifts (δ) for other branched PPEIs (1200, 2000) revealed a double peak in the range of 3.56−3.42 ppm. For the linear PPEI-5000, the doublet peak of the -N-C**H**$_2$-PO_3H_2- group is shown at δ 3.66−3.64 ppm. It is well known that the ^{31}P NMR technique is a potent procedure to confirm the chemical structure of most organophosphorus compounds. The ^{31}P NMR chemical shifts of branched PPEI-600, 1200, and 2000 were recorded at δ 18.33, 17.67, and 15.40 ppm, respectively. Furthermore, the ^{31}P NMR chemical shift of linear PPEI-5000 showed a significant peak at δ 19.78 ppm, corresponding to the phosphonate group (PO_3H_2) in the polymer structure backbone. Based on the above finding characterization results, we can conclude that all branched and linear PPEIs have been prepared successfully.

3.2. High-Pressure Scale Inhibition Tube-Blocking Experiments. The open literature states that LMW-PEI is not toxic and has been widely used as a gene delivery agent for many years.[41−45] This motivated us to phosphonate a series of branched and linear PEIs using the Moedritzer−Irani reaction to develop a new green class of phosphonate-based SIs (PPEIs) for the upstream oil and gas industry. Table 2 shows the scale inhibition efficiencies of all synthesized branched and linear LMW-PPEIs against the calcium carbonate scale (calcite) using a high-pressure dynamic tube-blocking rig at 100 °C and approximately 80 bar. In addition, the inhibition performances of these new SIs were compared with two commercial amino methylenephosphonate SIs, ATMP and DTPMP. In this study, the model fluids were used according to the Heidrun oilfield, Norway (Table 1). To check the repeatability of the experimental results, the whole test was repeated twice. In general, various concentrations of SIs (100−1 ppm) at pH 4−6 were flushed through pump 3 over the test period of 1 h until the mineral scale was produced in the coil at failed inhibition concentrations (FICs).

Table 2. Dynamic Calcite Scale Inhibition Experiments[a]

	calcite scale					
	first blank	first scale test		second scale test		second blank
SI (1000 ppm)	time (min)	conc. (ppm)	time (min)	conc. (ppm)	time (min)	time (min)
ATMP	11	20	26	20	26	12
DTPMP	10	10	20	10	20	12
branched PPEI-600	11	10	19	10	16	10
branched PPEI-1200	9	20	38	20	35	10
branched PPEI-2000	8	20	59	20	59	10
linear PPEI-5000	9	20	25	20	25	11

[a]The accuracy for all numerical values was ±5 min.

For commercial amino methylenephosphonate SIs, ATMP and DTPMP, showed a moderate inhibition performance against the calcite scale. ATMP gave an FIC of 20 ppm after 26 min in the first and repeat test. However, DTPMP displayed a slightly better calcite inhibition performance than ATMP under the same test conditions. The FIC of DTPMP was 10 ppm after 20 min for both experiments (Table 2).[68−70]

For branched PPEI SIs, it was found that all three modified polymers with ranges of low molecular weights exhibited a moderate dynamic scale inhibition performance for the calcite scale. However, the lower polymer molecular weight of the tested branched PPEIs has improved the calcite inhibition performance. Branched PPEI-600 gave better calcite inhibition performance than other branched and linear PPEIs. It was also found that branched PPEI-600 showed an efficiency similar to the commercial DTPMP SI. The FIC of branched PPE-600 was 10 ppm after 19 and 16 min for the first and second scale experiments under dynamic conditions (Table 2), respectively. Figure 5 presents a schematic diagram of a whole scale inhibition test of branched PPEI-600 against the calcium carbonate scale in a high-pressure dynamic tube-blocking rig at 100 °C and 80 bar. This diagram shows all four steps of the dynamic test for each SI as follows: (a) a blank test with no additives, (b) a test to implement the FIC, (c) a repeat FIC test, and (d) a repeat blank test. We have previously illustrated these stages in detail in our published articles.[68−70]

Branched PPEI-1200 and PPEI-2000 gave a weak inhibition performance with an FIC of 20 ppm compared to branched PPEI-600 and the commercial DTPMP SI. It was found that these branched PPEIs (12 000 and 2000) gave a similar inhibition efficiency to commercial ATMP (FIC = 20 ppm). Figure 6 shows the graphically obtained results of FIC and the scaling time for branched PPEI-2000 against the calcite scale. The FIC of PPEI-2000 was 20 ppm after 59 min for the first and repeat tests. Our speculation for this limited calcite inhibition efficiency for all branched PPEIs is their incompatibility with calcium ions. We assume that the presence of many amino methylenephosphonate groups on the SI backbone may lead to intolerance activity with calcium ions, affording the SI-Ca^{2+} complex.[68−70] The graphical slope in Figures 5 and 6 highlighted the intolerance activity of branched PPEIs with calcium ions, as investigated previously.[71]

https://doi.org/10.1021/acs.iecr.2c01730
Ind. Eng. Chem. Res. 2022, 61, 9586−9599

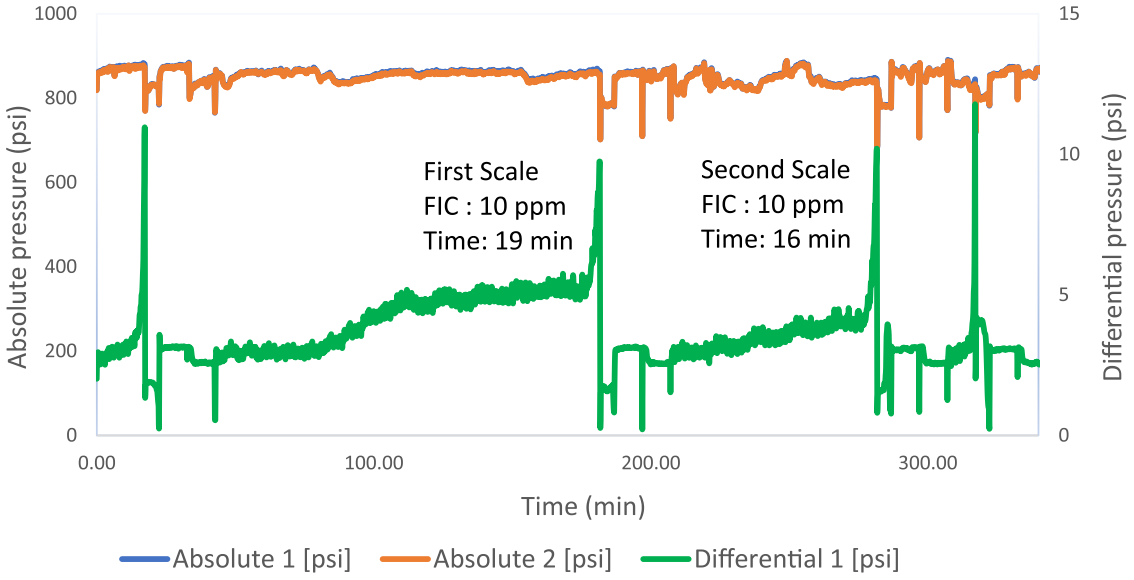

Figure 5. Schematic diagram of the calcium carbonate dynamic test for branched PPEI-600.

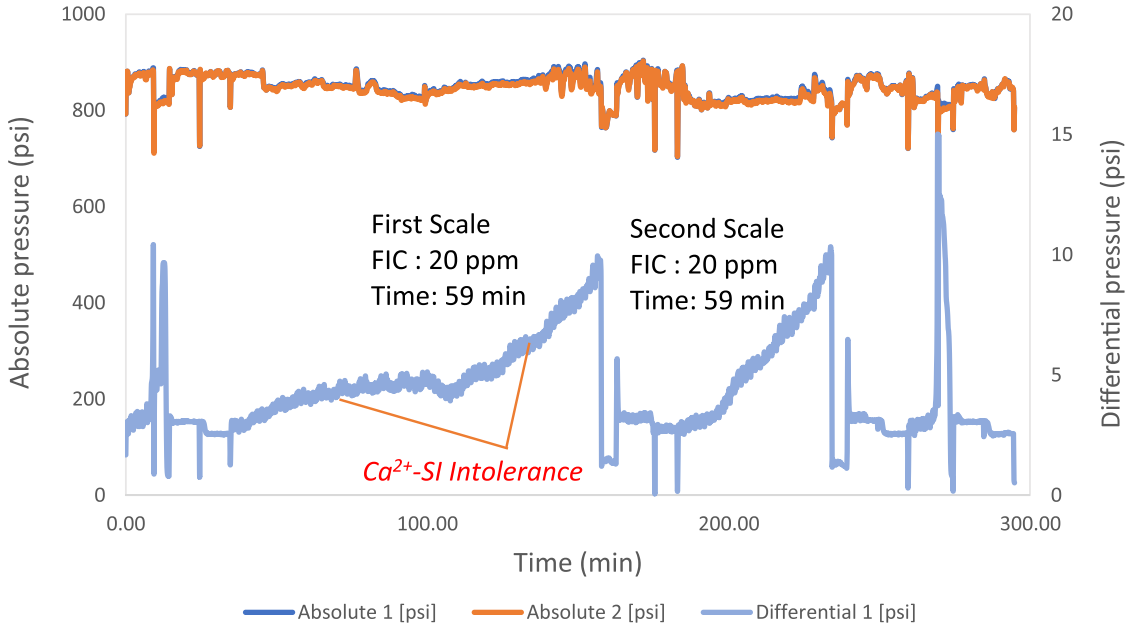

Figure 6. Schematic diagram of the calcium carbonate dynamic test for branched PPEI-2000.

Interestingly, our modified branched PPEIs via the Moedritzer−Irani reaction gave a better calcite inhibition performance than branched PPEIs (based on the -N-CH_2-CH_2-PO_3H_2 group) using the Michael addition synthetic route in the presence of a vinyl phosphonic monomer.[41] For example, the FIC of branched PPEI-1200 via the Moedritzer−Irani reaction was 20 ppm, while the FIC of branched PPEI-1200 via the Michael addition synthetic pathway was ≥240 ppm under the same dynamic test conditions.[41]

Linear PPEI-5000 also showed a moderate inhibition performance for the calcium carbonate scale at the same dynamic test conditions (100 °C, ca. 80 bar). It was found that linear PPEI-5000 failed at 20 ppm after 25 min for both experiments, as tabulated in Table 2. The graphical diagram of the dynamic calcite test for linear PPEI-5000 is presented in Figure 7. It was observed that there is no gradual increase in the differential pressure slope for linear PPEI-5000 compared to all branched PPEIs. This encouraged us to investigate the compatibility activity of all branched and linear PPEIs with calcium ions under various SI/Ca^{2+} concentrations. The calcium tolerance of all synthesized PPEIs will be discussed later in the calcium compatibility section.

Table 3 presents the FICs and scaling times for two commercial SIs, ATMP and DTPMP, and all new branched and linear PPEIs against the barium sulfate scale (barite) in a dynamic tube-blocking scale instrument at 100 °C and 80 bar. It was found that commercial amino methylenephosphonate SIs, ATMP and DTPMP, displayed good inhibition efficiency for barite scaling. For example, the FIC of DTPMP was 5 ppm after 5 min for the first scale test and 9 min for the second scale test (Table 3). It is well known that the number of phosphonate groups in the inhibitor backbone plays a remarkable role in oilfield barite prevention. -Bromley et al. reported that the SI with more than one phosphonate moiety

https://doi.org/10.1021/acs.iecr.2c01730
Ind. Eng. Chem. Res. 2022, 61, 9586−9599

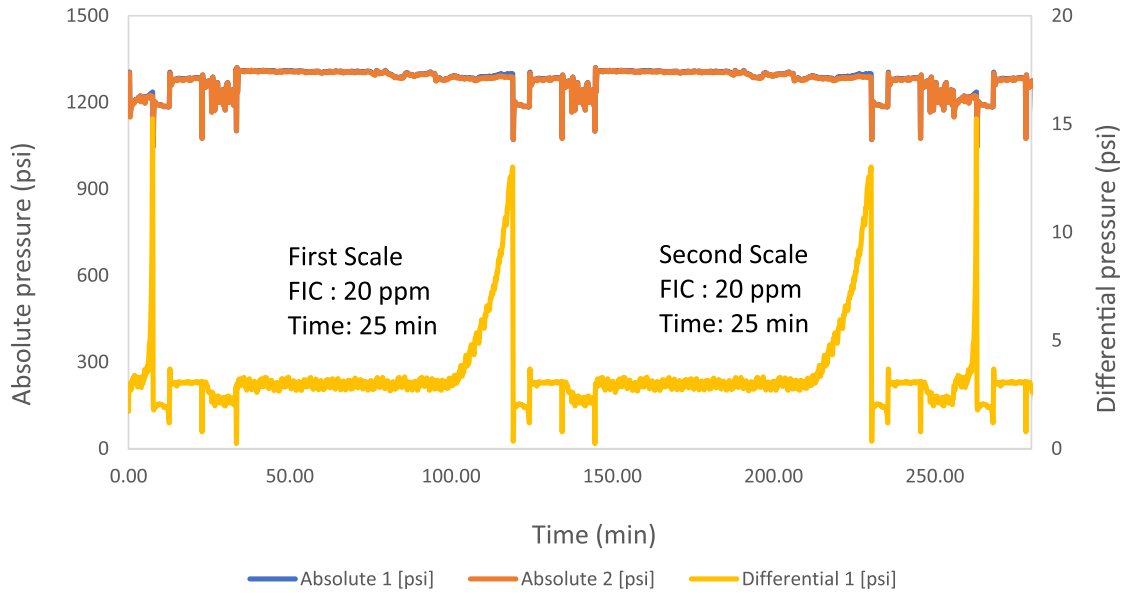

Figure 7. Schematic diagram of the calcium carbonate dynamic test for linear PPEI-5000.

Table 3. Dynamic Barite Scale Inhibition Experiments[a]

	barite scale					
	first blank	first scale test		second scale test		second blank
SI (1000 ppm)	time (min)	conc. (ppm)	time (min)	conc. (ppm)	time (min)	time (min)
ATMP	11	10	42	10	41	11
DTPMP	10	5	5	5	9	10
branched PPEI-600	10	20	38	20	33	11
branched PPEI-1200	10	20	59	20	58	11
branched PPEI-2000	10	20	15	20	13	11
Linear PPEI-5000	10	50	46	50	40	11

[a]Accuracy for all numerical values was ±5 min.

increased the active sites of the phosphonate binding surface, affording greatly improved barite prevention.[72] Therefore, DTPMP (including 5 phosphonate groups) gave good barite scaling inhibition performance compared to ATMP (including 3 phosphonate groups), as shown in Table 3.

Branched PPEIs showed a moderate inhibition performance against barite scaling. These compounds gave an FIC of 20 ppm in the first and repeat tests. Figure 8 presents the schematic diagram of the branched PPEI-600 against barite scaling. The FIC was 20 ppm after 38 and 33 min for the first and second dynamic scaling tests, respectively. It was also investigated that our synthesized branched PPEIs under the Moedritzer−Irani conditions showed better barite inhibition efficiency compared to branched PPEIs utilizing the Michael addition reaction.[41] For example, branched PPEI-1200 (based on the Moedritzer−Irani reaction) failed at 20 ppm for both runs, and PPEI-1200 (based on the Michael addition reaction) failed at ≥500 ppm.[41] We speculate that the significant reason for this moderate efficiency against barite scaling is the high degree of branching PPEI in which the inhibitor curled up in more compact conformations. Furthermore, linear PPEI-5000

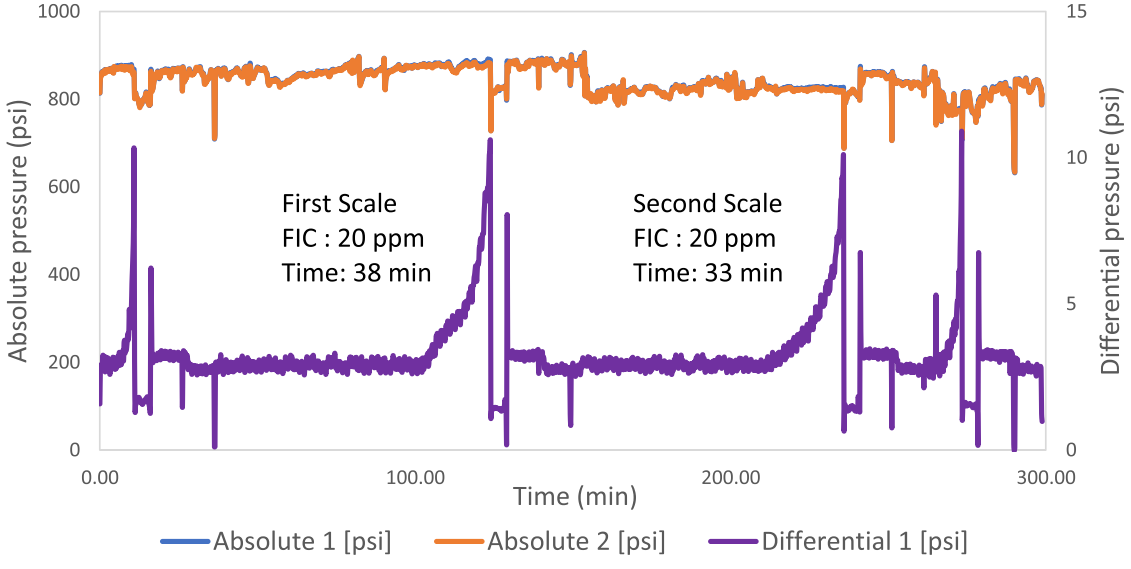

Figure 8. Schematic diagram of the barium sulfate dynamic test for branched PPEI-600.

https://doi.org/10.1021/acs.iecr.2c01730
Ind. Eng. Chem. Res. 2022, 61, 9586−9599

Table 4. Tolerance Experiments in 10 000 ppm of Ca^{2+} and 30 000 ppm (3.0 wt %) of NaCl for Branched PPEI-600

	appearance				
dose (ppm)	at mixing	30 min	1 h	4 h	24 h
100	clear	clear	clear	clear	clear
1000	clear	haze	haze	haze	haze
10 000	haze	precipitated	precipitated	precipitated	precipitated
50 000	haze	precipitated	precipitated	precipitated	precipitated

showed the worst barite inhibition efficiency than commercial SIs and branched PPEIs (Table 3). The FIC was 50 ppm after 46 and 40 min for both runs, respectively. We assume the main reason for this weak performance of linear PPEI compared to branched PPEIs is the lack of enough phosphonate groups in the SI backbone to mitigate the barite scale formation.

3.3. Calcium Compatibility Test. Amino methylene-phosphonate-based SIs are widely used in the oil and gas industry. However, most of these products are incompatible with high calcium ions in the oilfield formation water and/or seawater. This intolerance behavior between SI and Ca^{2+} ions may lead to the formation of SI-Ca^{2+} complex precipitate. If the SI is deployed for squeeze treatment application, it could cause formation damage in the petroleum reservoir. Therefore, we have studied the compatibility activity between all branched and linear PPEIs and calcium ions at different concentrations. For branched PPEIs, it was found that all branched PPEIs gave moderate to poor calcium compatibility activities (Tables S1 and S2). It was found that all branched PPEIs at 100 ppm were only compatible with 100 ppm of Ca^{2+} ions over the test period (24 h). However, high concentrations of calcium ions (1000 and 10 000 ppm) were incompatible with all tested branched PPEI SI concentrations (1000−50 000 ppm). For example, Table 4 shows the results of calcium tolerance for branched PPEI-600 (100−50 000 ppm) in 10000 ppm of calcium ions. Hazy solutions and deposits were recorded in 1000−50 000 ppm of branched PPEI-600, as shown in Figure 9a. As investigated earlier, the graphical slope in the obtained

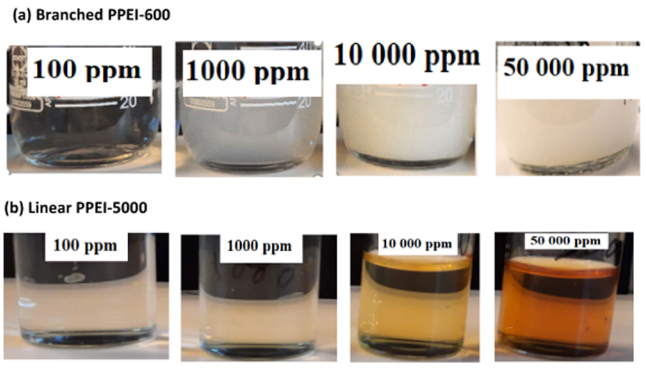

Figure 9. Appearance of calcium tolerance tests of branched and linear PPEIs (100−50 000 ppm) after 24 h in 10 000 ppm of calcium ions (a) branched PPEI-600 and (b) linear PPEI-5000.

figures of dynamic calcite experiments (Figures 5 and 6) pointed out that these branched PPEIs are incompatible with Ca^{2+} ions. These findings of calcium compatibility results are correlated with the weak performance of the branched PPEIs.

On the contrary, linear PPEI-5000 gave outstanding calcium compatibility at all inhibitor concentrations and calcium ions (up to 10 000 ppm). Table 5 and Figure 9b present the extreme matrix of linear PPEI-5000 (up to 50 000 ppm) at a

Table 5. Tolerance Experiments in 10 000 ppm of Ca^{2+} and 30 000 ppm (3.0 wt %) of NaCl for Linear PPEI-5000

	appearance				
dose (ppm)	at mixing	30 min	1 h	4 h	24 h
100	clear	clear	clear	clear	clear
1000	clear	clear	clear	clear	clear
10 000	clear	clear	clear	clear	clear
50 000	clear	clear	clear	clear	clear

high concentration of Ca^{2+} ions of 10 000 ppm. No haziness or depositions were recorded over the test period of 24 h. Our explanation for this superior calcium compatibility performance is the presence of a few phosphonate groups in the linear structure backbone, avoiding the formation of the Ca^{2+}-SI complex.

3.4. Crystal Morphology Analysis. Figure 10 shows the SEM images of the Heidrun calcium carbonate scale crystals in the presence and absence of linear PPEI-5000. It was observed that SEM images of Heidrun calcite crystals in the absence of the inhibiting polymer PPEIs are presented in cubic-shaped blocks with smooth and compact surfaces, which are typical of calcite crystals (Figure 10a).[73] These cubical-shaped blocks of the Heidrun calcite crystals have been distorted and significantly changed in the presence of the inhibiting polymer. For example, at 10 ppm of linear PPEI-5000 SI, the $CaCO_3$ crystals become rod-shaped (needle-shaped crystallites), as shown in Figure 10b. It was also observed that the diameter of the crystals is shorter than that of the untreated crystals. At higher dosages of linear PPEI-5000 SI (100 ppm), the crystals are completely turned into an irregular form, affording long cluster shapes (Figure 10c,d). Moreover, Figure S1 presents the SEM images of the crystal of the neat Heidrun barite scale, as well as the barite crystal with 100 ppm of linear PPEI-5000. It was found that the morphology of the barite crystal was completely changed from a starlike structure to a thin thread shape in the presence of 100 ppm of linear PPEI-5000, as shown in Figure S1b.

We can conclude that the inhibiting phosphonate group in the SI backbone was successfully adsorbed onto the active sites of the calcium carbonate and barium sulfate crystal surfaces, leading to a calcite and barite lattice distortion, thus preventing the crystallization.

3.5. Density Functional Theory Simulations. Solid-state DFT simulations are carried out to get atomic insights into the adsorption of the PPEI polymer on the most stable facet of calcite (104) and barite (001). We have calculated the adsorption energies of PPEI linear and branched repeating units on the mineral facet (Figures 11 and S2) and compared them with those of commercial inhibitors such as ATMP to assess their performance. The results in Table 6 indicate that linear and branched PPEI polymers display a favorable interaction with the mineral facet of calcite and barite with more affinities toward calcite. We have modeled the linear

https://doi.org/10.1021/acs.iecr.2c01730
Ind. Eng. Chem. Res. 2022, 61, 9586−9599

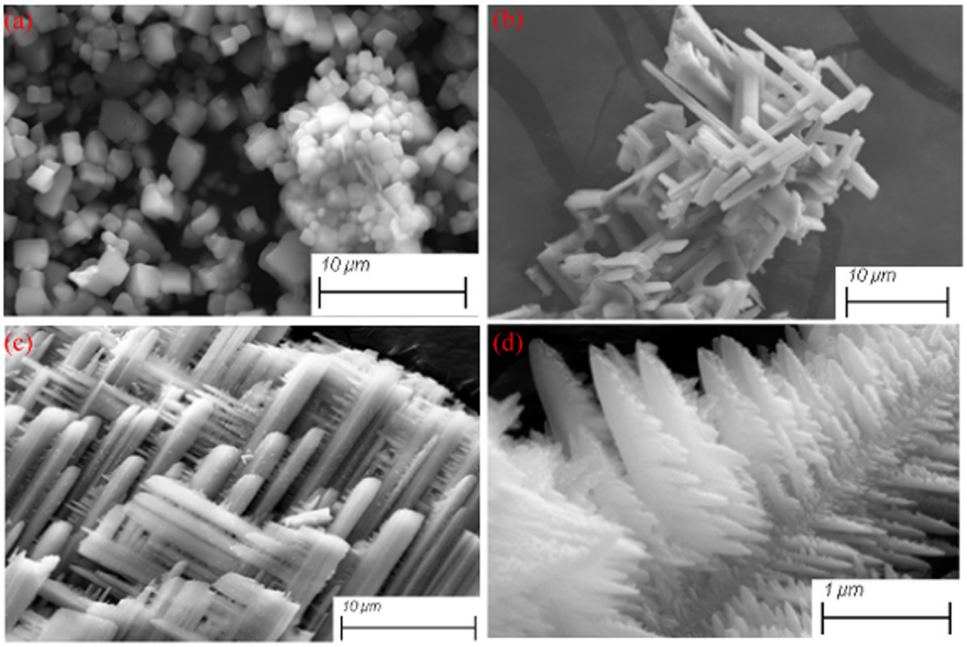

Figure 10. SEM images of the Heidrun calcium carbonate scale: (a) neat $CaCO_3$; (b) $CaCO_3$, with 10 ppm of linear PPEI-5000—scale bar 10 μm; (c) $CaCO_3$, with 100 ppm of linear PPEI-5000—scale bar 10 μm; and (d) $CaCO_3$, with 100 ppm of linear PPEI-5000—scale bar 1 μm.

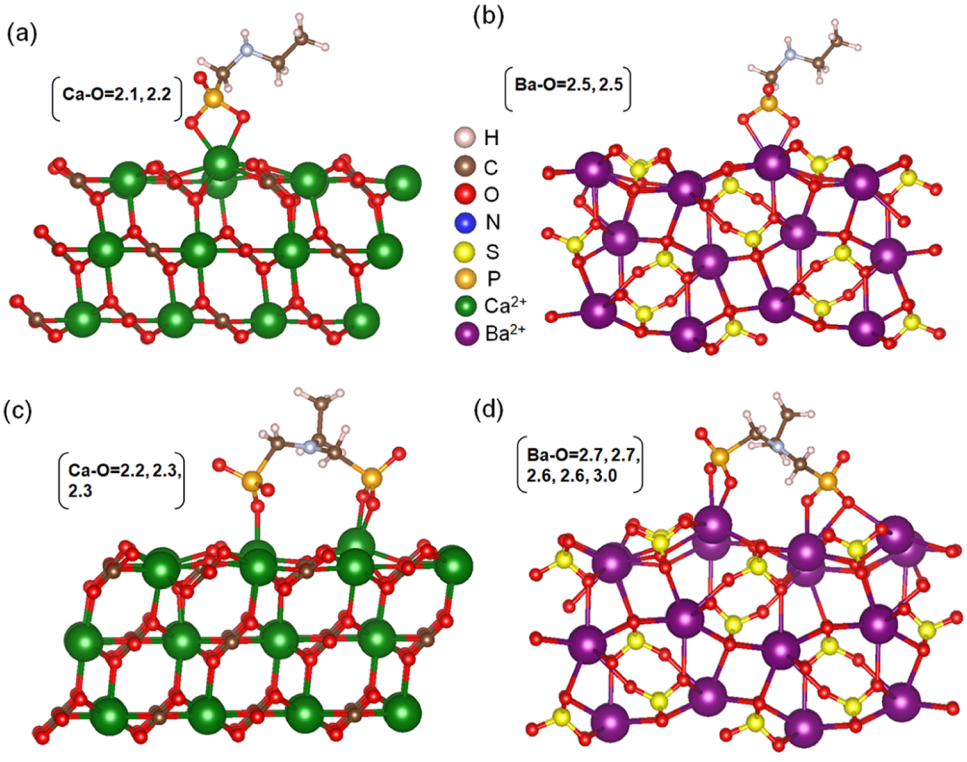

Figure 11. Optimized structures of PPEI linear and branched on calcite (a, c) and barite (b,d). Key bond lengths are shown in Å, and the atomic color code is presented.

Table 6. Adsorption Energies of PPEI Monomers on Calcite and Barite Facets Are Reported in eV. The Phosphonate Groups Are Considered Deprotonated

SIs	calcite (104)	barite (010)
PPEI-L	−3.2	−0.75
PPEI-B	−10.2	−9.4
ATMP	−16.0	−11.57[74]

PPEI with one phosphonate group and the branched with two phosphonates to reflect the density of the functional group of the two polymers. It is evident from the results that the higher the number of phosphonates, the stronger the interactions with the mineral facets. The branched PPEI displays affinity close to that reported of ATMP for the calcite and barite. We also calculated the adsorption energies with the phosphonate groups monoprotonated (Table S3) and found that they

https://doi.org/10.1021/acs.iecr.2c01730
Ind. Eng. Chem. Res. 2022, 61, 9586−9599

exhibit lower affinities than the deprotonated form. The interaction of PPEI polymers with displaying coordinating bonds shorter with the calcite facet than with the barite is due to the morphology difference between the two minerals. The phosphonate groups exhibit electrostatic repulsion, with the tetrahedral sulfate group on the barite surface stronger than the linear carbonate groups on the calcite surface.

The difference in the performance of PPEI polymers against calcite and barite could be related to the intrinsic kinetics of the scale formations of the two minerals and the polymer morphology. The sluggish barite kinetics of barite, which involves amorphous particles that undergo slow transformation to the crystalline morphology, requires a higher polymer concentration to inhibit the scale compared to the calcite scale.[75] In addition, the higher density of phosphonate groups and their random distributions makes the polymer−mineral interaction mechanism more complicated to predict.

Furthermore, we have performed a molecular metal-binding energy calculation of Ca^{2+} with one unit of the branched PPEI to estimate its calcium affinity (Figure S3). Such an estimation will help to understand the calcium compatibility of PPEI polymers. The calculated Ca^{2+} binding was −59.73 kcal/mol, which is less than DTPMP (−75.85) and higher than ATMP (−53.53 kcal/mol) considering the protonation states of the three molecules. The strong calcium affinities of the PPEI polymer explain its poor calcium compatibility. In addition, the high density of the phosphonate groups distributed on the branched PPEI polymer could result in calcium condensation and polymer flocculation.

DFT simulations predicted that PPEI displays a good affinity for the calcite and barite facets. However, the scale kinetics and polymer morphology make the mineral−polymer interaction mechanism challenging to predict. The calcium affinity of the PPEI unit explains its poor calcium compatibility because the strong interactions between calcium and phosphonate could result in high ion condensation on the polymer surface and in turn, the polymer flocculation.

4. CONCLUSIONS

Given that low-molecular-weight polyethyleneimine (LMW-PEI) is low toxic, a series of branched and linear amino methylenephosphonate-based PEIs have been developed as new scale inhibitors for the upstream oil and gas industry. All branched and linear phosphonated polyethyleneimines (PPEIs) were synthesized via the Moedritzer−Irani reaction. The presented branched PPEIs are named branched PPEI-600, branched PPEI-1200, and branched PPEI-2000, while the corresponding linear PPEI is labeled linear PPEI-5000. The branched and linear PPEIs have been compared and screened with two commercial amino methylenephosphonate SIs, ATMP and DTPMP, through high-pressure dynamic tube-blocking inhibition and calcium compatibility tests. In addition, the morphology of the calcium carbonate and barium sulfate scale crystals in the absence and presence of linear PPEI-5000 was also investigated using scanning electron microscopy (SEM). Quantum chemical simulations for branched and linear PPEIs were conducted to get atomic insights into the polymer-scale interactions. The major conclusions are listed as follows:

(1) All branched PPEIs (M_w = 600, 1200, and 2000) exhibited a moderate calcite dynamic scale inhibition performance. It was found that the lower polymer molecular weight of the tested branched PPEIs has improved the calcite inhibition performance. Branched PPEI-600 gave better calcite inhibition performance than other branched and linear PPEIs. The FIC of branched PPEI-600 was 10 ppm, while the FICs of branched PPEIs-1200 and 2000 were 20 ppm. It was also found that the amino methylenephosphonate-based PEI gave a much better scale inhibition performance than the amino ethylenephosphonate-based PEI for calcite and barite scales.

(2) All branched and linear PPEIs showed a moderate barite dynamic scale inhibition performance. The FICs of all branched PPEIs were 20 ppm, while the FIC of linear PPEI-5000 was 50 ppm.

(3) The branched PPEIs gave moderate to poor calcium compatibility at high dosages of calcium ions (1000−10 000 ppm). Interestingly, linear PPEI- 5000 displayed superior compatibility properties at high dosages of SI (up to 50 000 ppm) and high concentrations of Ca^{2+} ions (up to 10 000 ppm).

(4) The field emission scanning electron microscopy analysis confirmed that the crystal shapes of $CaCO_3$ and $BaSO_4$ mineral scales are significantly changed in the presence of linear PPEI-5000. At high dosages of linear PPEI-5000 SI (100 ppm), the $CaCO_3$ crystals are completely converted from cubic-shaped blocks (blank calcite) into long cluster shapes. This confirms that the inhibiting phosphonate moiety in the inhibitor chain was successfully adsorbed onto the calcite surface active sites, affording lattice distortion, thus inhibiting crystallization.

(5) DFT simulations predict that the linear and branched PPEI polymers exhibit a favorable interaction with the two mineral facets with more affinities toward calcite, supporting SEM results.

(6) The complicated polymer morphology and the scale formation kinetics make the polymer inhibition mechanism challenging to predict.

We are currently studying the toxicity and thermal stability properties of branched PPEI-600 and linear PPEI-5000 to check their ability for squeeze treatment application. In addition, we plan to investigate their adsorption/desorption activities on formation rock using the core-flooding technique for use in squeeze treatments.

■ ASSOCIATED CONTENT

Supporting Information

The Supporting Information is available free of charge at https://pubs.acs.org/doi/10.1021/acs.iecr.2c01730.

(Table S1) Ca^{2+} tolerance tests at 30000 ppm (3 wt%) NaCl for branched PPEIs (M_w = 600, 1200, and 2000) and linear PPEI-5000; (Table S2) calcium tolerance tests: appearance after 24 hours; (Table S3) adsorption energies of PPEI monomers on calcite and barite facets are reported in eV; phosphonated groups considered monoprotonated; (Table S4) pH values of all tested PPEI SIs against the oilfield scale; (Table S5) salts used to make brines 1 and 2 for calcite scaling; (Table S6) salts used to make brines 1 and 2 for barite scaling; (Figure S1) SEM images of the Heidrun barium sulfate scale: (a) neat $BaSO_4$ and (b) $BaSO_4$, with 100 ppm of linear PPEI-5000—scale bar 10 μm; and (Figure S2) optimized structures of PPEI linear and branched on

https://doi.org/10.1021/acs.iecr.2c01730
Ind. Eng. Chem. Res. 2022, 61, 9586−9599

calcite (a, c) and on barite (b,d). Key bond lengths are shown in Å and the atomic color code is presented. Phosphonate groups are considered monoprotonated and (Figure S3) the PPEI-Ca^{2+} complex with coordination bonds reported in angstrom (PDF)

AUTHOR INFORMATION

Corresponding Author

Mohamed F. Mady − *Department of Chemistry, Bioscience and Environmental Engineering, Faculty of Science and Technology, University of Stavanger, N-4036 Stavanger, Norway; Department of Green Chemistry, National Research Centre, Giza, Cairo 12622, Egypt;* orcid.org/0000-0002-4636-0066; Email: mohamed.mady@uis.no

Authors

Ali H. Karaly − *Department of Chemistry, Bioscience and Environmental Engineering, Faculty of Science and Technology, University of Stavanger, N-4036 Stavanger, Norway;* orcid.org/0000-0002-1711-5862

Safwat Abdel-Azeim − *Center of Integrative Petroleum Research (CIPR), College of Petroleum and Geosciences (CPG), King Fahd University of Petroleum and Minerals, Dhahran 31261, Saudi Arabia;* orcid.org/0000-0001-8611-1251

Ibnelwaleed A. Hussein − *Gas Processing Center, College of Engineering, Qatar University, Doha, Qatar; Department of Chemical Engineering, College of Engineering, Qatar University, Cairo 12622, Egypt;* orcid.org/0000-0002-6672-8649

Malcolm A. Kelland − *Department of Chemistry, Bioscience and Environmental Engineering, Faculty of Science and Technology, University of Stavanger, N-4036 Stavanger, Norway;* orcid.org/0000-0003-2295-5804

Ahmed Younis − *Department of Green Chemistry, National Research Centre, Giza, Cairo 12622, Egypt*

Complete contact information is available at: https://pubs.acs.org/10.1021/acs.iecr.2c01730

Notes

The authors declare no competing financial interest.

ACKNOWLEDGMENTS

Financial support from the Research Council of Norway and the University of Stavanger for Green Production Chemistry Based Nanotechnology (the PETROMAKS 2 programme, Research Project No. 300754) is gratefully acknowledged. S.A.A. thanks the Supercomputer Shaheen at King Abdullah University of Science & Technology (KAUST) in Thuwal, Saudi Arabia, for allowing usage of its computational resources.

REFERENCES

(1) Mady, M. F. Chapter 16 - Oilfield Scale Inhibitors: Synthetic and Performance Aspects. In *Water-Formed Deposits*; Amjad, Z.; Demadis, K. D., Eds.; Elsevier, 2022; pp 325−352, DOI: 10.1016/B978-0-12-822896-8.00033-9.

(2) Gudmundsson, J. S. *Flow Assurance Solids in Oil and Gas Production*; CRC Press: London, 2017, DOI: 10.1201/9781315185118.

(3) Amjad, Z. *The Science and Technology of Industrial Water Treatment*; CRC press, 2010.

(4) Kelland, M. A. *Production Chemicals for the Oil and Gas Industry*; CRC press, 2016.

(5) Frenier, W. W.; Ziauddin, M. *Formation, Removal, and Inhibition of Inorganic Scale in the Oilfield Environment*; Society of Petroleum Engineers Richardson: TX, 2008.

(6) Atkinson, G.; Mecik, M. The Chemistry of Scale Prediction. *J. Pet. Sci. Eng.* **1997**, *17*, 113−121.

(7) Van Driessche, A. E. S.; Benning, L. G.; Rodriguez-Blanco, J. D.; Ossorio, M.; Bots, P.; García-Ruiz, J. M. The Role and Implications of Bassanite as a Stable Precursor Phase to Gypsum Precipitation. *Science* **2012**, *336*, 69−72.

(8) Chen, T.; Honarparvar, S.; Reible, D.; Chen, C.-C. Thermodynamic Modeling of Calcium Carbonate Scale Precipitation: Aqueous Na+-Ca2+-Cl−-HCO3−-CO32−-CO2 System. *Fluid Phase Equilib.* **2022**, *552*, No. 113263.

(9) Scale Prediction for Oil and Gas Production | SPE Journal | OnePetro. https://onepetro.org/SJ/article/17/02/362/198122 (accessed March 31, 2022).

(10) Fan, C.; Kan, A. T.; Zhang, P.; Lu, H.; Work, S.; Yu, J.; Tomson, M. B. Scale Prediction and Inhibition for Oil and Gas Production at High Temperature/High Pressure. *SPE J.* **2012**, *17*, 379−392.

(11) Amjad, Z.; Demadis, K. D. *Mineral Scales and Deposits: Scientific and Technological Approaches*; Elsevier, 2015.

(12) Crabtree, M.; Eslinger, D.; Fletcher, P.; Miller, M.; Johnson, A.; King, G. Fighting Scale-Removal and Prevention. In *Oil Field Review*; Elsevier, Amsterdam: Netherlands, 1999; Vol. *11*, pp 30−45.

(13) Jafar Mazumder, M. A. A Review of Green Scale Inhibitors: Process, Types, Mechanism and Properties. *Coatings* **2020**, *10*, No. 928.

(14) Xu, J.; Jing, G.; Liu, T.; Liu, Y.; Yanheng, L.; Yang, Y. Research Progress of Green Scale Inhibitors: A Mini Review. *Pet. Sci. Technol.* **2022**, *40*, 59−72.

(15) Mady, M. F.; Kelland, M. A. Overview of the Synthesis of Salts of Organophosphonic Acids and Their Application to the Management of Oilfield Scale. *Energy Fuels* **2017**, *31*, 4603−4615.

(16) Dyer, S. J.; Anderson, C. E.; Graham, G. M. Thermal Stability of Amine Methyl Phosphonate Scale Inhibitors. *J. Pet. Sci. Eng.* **2004**, *43*, 259−270.

(17) Dyer, S. J.; Graham, G. M.; Sorbie, K. S. Factors Affecting the Thermal Stability of Conventional Scale Inhibitors for Application in High Pressure/High Temperature Reservoirs. In *OnePetro*, 1999, DOI: 10.2118/50717-MS.

(18) Commission, O. Guidelines for Completing the Harmonised Offshore Chemical Notification Format (HOCNF), Agreement 2012-05, OSPAR Commission, London, 2015.

(19) Hasson, D.; Shemer, H.; Sher, A. State of the Art of Friendly "Green" Scale Control Inhibitors: A Review Article. *Ind. Eng. Chem. Res.* **2011**, *50*, 7601−7607.

(20) Mady, M. F.; Kelland, M. A. Study on Various Readily Available Proteins as New Green Scale Inhibitors for Oilfield Scale Control. *Energy Fuels* **2017**, *31*, 5940−5947.

(21) Mady, M. F.; Rehman, A.; Kelland, M. A. Synthesis and Study of Modified Polyaspartic Acid Coupled Phosphonate and Sulfonate Moieties As Green Oilfield Scale Inhibitors. *Ind. Eng. Chem. Res.* **2021**, *60*, 8331−8339.

(22) Mady, M. F.; Malmin, H.; Kelland, M. A. Sulfonated Nonpolymeric Aminophosphonate Scale Inhibitors-Improving the Compatibility and Biodegradability. *Energy Fuels* **2019**, *33*, 6197−6204.

(23) Mady, M. F.; Bayat, P.; Kelland, M. A. Environmentally Friendly Phosphonated Polyetheramine Scale Inhibitors-Excellent Calcium Compatibility for Oilfield Applications. *Ind. Eng. Chem. Res.* **2020**, *59*, 9808−9818.

(24) Demeneix, B.; Behr, J. Polyethylenimine (PEI). In *Advances in Genetics; Non-Viral Vectors for Gene Therapy*, 2nd ed.; Academic Press, 2005; Vol. 53, Part 1, pp 215−230 DOI: 10.1016/S0065-2660(05)53008-6.

(25) Polyethyleneimine - An Overview | ScienceDirect Topics. https://www.sciencedirect.com/topics/medicine-and-dentistry/polyethyleneimine (accessed April 01, 2022).

(26) Vicennati, P.; Giuliano, A.; Ortaggi, G.; Masotti, A. Polyethylenimine In Medicinal Chemistry. *Curr. Med. Chem.* **2008**, *15*, 2826−2839.
(27) Yan, D.; Gao, C.; Frey, H. *Hyperbranched Polymers: Synthesis, Properties, and Applications*; John Wiley & Sons, 2011.
(28) Remy, J.-S.; Abdallah, B.; Zanta, M. A.; Boussif, O.; Behr, J.-P.; Demeneix, B. Gene Transfer with Lipospermines and Polyethylenimines. *Adv. Drug Delivery Rev.* **1998**, *30*, 85−95.
(29) Lahrouch, F.; Sofronov, O.; Creff, G.; Rossberg, A.; Hennig, C.; Den Auwer, C.; Di Giorgio, C. Polyethyleneimine Methylphosphonate: Towards the Design of a New Class of Macromolecular Actinide Chelating Agents in the Case of Human Exposition. *Dalton Trans.* **2017**, *46*, 13869−13877.
(30) Takagishi, T.; Okuda, S.; Kuroki, N.; Kozuka, H. Binding of Metal Ions by Polyethylenimine and Its Derivatives. *J. Polym. Sci., Polym. Chem. Ed.* **1985**, *23*, 2109−2116.
(31) Archer, W. R.; Fiorito, A.; Heinz-Kunert, S. L.; MacNicol, P. L.; Winn, S. A.; Schulz, M. D. Synthesis and Rare-Earth-Element Chelation Properties of Linear Poly (Ethylenimine Methylenephosphonate). *Macromolecules* **2020**, *53*, 2061−2068.
(32) Navarro, R. R.; Wada, S.; Tatsumi, K. Heavy Metal Precipitation by Polycation−Polyanion Complex of PEI and Its Phosphonomethylated Derivative. *J. Hazard. Mater.* **2005**, *123*, 203−209.
(33) Navarro, R. R.; Wada, S.; Tatsumi, K. Heavy Metal Flocculation by Phosphonomethylated-Polyethyleneimine and Calcium Ions. *Sep. Sci. Technol.* **2003**, *38*, 2327−2345.
(34) Villemin, D.; Monteil, C.; Bar, N.; Didi, M. A. Phosphonated Polyethyleneimines (PEIP) as Multi-Use Polymers. *Phosphorus, Sulfur Silicon Relat. Elem.* **2015**, *190*, 879−890.
(35) Navarro, R. R.; Tatsumi, K. Enhancement of Phosphonomethylated PEI−Cu2+ Complex Flocculation by Ca2+ Ions: A New Approach for Heavy Metal Removal from Aqueous Solutions. *Sep. Sci. Technol.* **2002**, *37*, 203−216.
(36) Demadis, K. D.; Preari, M.; Antonakaki, I. Naturally Derived and Synthetic Polymers as Biomimetic Enhancers of Silicic Acid Solubility in (Bio)Silicification Processes. *Pure Appl. Chem.* **2014**, *86*, 1663−1674.
(37) Spinthaki, A.; Skordalou, G.; Stathoulopoulou, A.; Demadis, K. D. Modified Macromolecules in the Prevention of Silica Scale. *Pure Appl. Chem.* **2016**, *88*, 1037−1047.
(38) Papathanasiou, K. E.; Vassaki, M.; Spinthaki, A.; Alatzoglou, F.-E. G.; Tripodianos, E.; Turhanen, P.; Demadis, K. D. Phosphorus Chemistry: From Small Molecules, to Polymers, to Pharmaceutical and Industrial Applications. *Pure Appl. Chem.* **2019**, *91*, 421−441.
(39) Wiesbrock, F.; Hoogenboom, R.; Leenen, M. A.; Meier, M. A.; Schubert, U. S. Investigation of the Living Cationic Ring-Opening Polymerization of 2-Methyl-, 2-Ethyl-, 2-Nonyl-, and 2-Phenyl-2-Oxazoline in a Single-Mode Microwave Reactor. *Macromolecules* **2005**, *38*, 5025−5034.
(40) Antonietti, L.; Aymonier, C.; Schlotterbeck, U.; Garamus, V. M.; Maksimova, T.; Richtering, W.; Mecking, S. Core- Shell-Structured Highly Branched Poly (Ethylenimine Amide) s: Synthesis and Structure. *Macromolecules* **2005**, *38*, 5914−5920.
(41) Godbey, W. T.; Wu, K. K.; Mikos, A. G. Size Matters: Molecular Weight Affects the Efficiency of Poly (Ethylenimine) as a Gene Delivery Vehicle. *J. Biomed. Mater. Res.* **1999**, *45*, 268−275.
(42) Kunath, K.; von Harpe, A.; Fischer, D.; Petersen, H.; Bickel, U.; Voigt, K.; Kissel, T. Low-Molecular-Weight Polyethylenimine as a Non-Viral Vector for DNA Delivery: Comparison of Physicochemical Properties, Transfection Efficiency and in Vivo Distribution with High-Molecular-Weight Polyethylenimine. *J. Controlled Release* **2003**, *89*, 113−125.
(43) Forrest, M. L.; Koerber, J. T.; Pack, D. W. A Degradable Polyethylenimine Derivative with Low Toxicity for Highly Efficient Gene Delivery. *Bioconjugate Chem.* **2003**, *14*, 934−940.
(44) Wen, Y.; Pan, S.; Luo, X.; Zhang, X.; Zhang, W.; Feng, M. A Biodegradable Low Molecular Weight Polyethylenimine Derivative as Low Toxicity and Efficient Gene Vector. *Bioconjugate Chem.* **2009**, *20*, 322−332.
(45) Thomas, T. J.; Tajmir-Riahi, H.-A.; Pillai, C. K. S. Biodegradable Polymers for Gene Delivery. *Molecules* **2019**, *24*, No. 3744.
(46) Moedritzer, K.; Irani, R. R. The Direct Synthesis of α-Aminomethylphosphonic Acids. Mannich-Type Reactions with Orthophosphorous Acid. *J. Org. Chem.* **1966**, *31*, 1603−1607.
(47) Mady, M. F.; Ortega, R.; Kelland, M. A. Exploring Modified Alendronic Acid as a New Inhibitor for Calcium-Based Oilfield Scales. *Energy Fuels* **2022**, *36*, 1863−1873.
(48) Mady, M. F.; Ortega, R. Fosfomycin and Its Derivatives: New Scale Inhibitors for Oilfield Applications. *ACS Omega* **2022**, *7*, 10701−10708.
(49) Kresse, G.; Hafner, J. Ab Initio Molecular Dynamics for Liquid Metals. *Phys. Rev. B: Condens. Matter Mater. Phys.* **1993**, *47*, No. 558.
(50) Kresse, G.; Hafner, J. Ab Initio Molecular-Dynamics Simulation of the Liquid-Metal−Amorphous-Semiconductor Transition in Germanium. *Phys. Rev. B: Condens. Matter Mater. Phys.* **1994**, *49*, No. 14251.
(51) Blöchl, P. E. Projector Augmented-Wave Method. *Phys. Rev. B: Condens. Matter Mater. Phys.* **1994**, *50*, No. 17953.
(52) Monkhorst, H. J.; Pack, J. D. Special Points for Brillouin-Zone Integrations. *Phys. Rev. B: Condens. Matter Mater. Phys.* **1976**, *13*, No. 5188.
(53) Perdew, J. P.; Burke, K.; Ernzerhof, M. Generalized Gradient Approximation Made Simple. *Phys. Rev. Lett.* **1996**, *77*, No. 3865.
(54) Grimme, S. Semiempirical GGA-Type Density Functional Constructed with a Long-Range Dispersion Correction. *J. Comput. Chem.* **2006**, *27*, 1787−1799.
(55) Bano, A. M.; Rodger, P. M.; Quigley, D. New Insight into the Stability of CaCO3 Surfaces and Nanoparticles via Molecular Simulation. *Langmuir* **2014**, *30*, 7513−7521.
(56) Jones, F.; Richmond, W. R.; Rohl, A. L. Molecular Modeling of Phosphonate Molecules onto Barium Sulfate Terraced Surfaces. *J. Phys. Chem. B* **2006**, *110*, 7414−7424.
(57) Mady, M. F.; Abdel-Azeim, S.; Kelland, M. A. Antiscaling Evaluation and Quantum Chemical Studies of Nitrogen-Free Organophosphorus Compounds for Oilfield Scale Management. *Ind. Eng. Chem. Res.* **2021**, *60*, 12175−12188.
(58) Chai, J.-D.; Head-Gordon, M. Systematic Optimization of Long-Range Corrected Hybrid Density Functionals. *J. Chem. Phys.* **2008**, *128*, No. 084106.
(59) Weigend, F.; Ahlrichs, R. Balanced Basis Sets of Split Valence, Triple Zeta Valence and Quadruple Zeta Valence Quality for H to Rn: Design and Assessment of Accuracy. *Phys. Chem. Chem. Phys.* **2005**, *7*, 3297−3305.
(60) Weigend, F. Accurate Coulomb-Fitting Basis Sets for H to Rn. *Phys. Chem. Chem. Phys.* **2006**, *8*, 1057−1065.
(61) Scalmani, G.; Frisch, M. J. Continuous Surface Charge Polarizable Continuum Models of Solvation. I. General Formalism. *J. Chem. Phys.* **2010**, *132*, No. 114110.
(62) Marenich, A. V.; Cramer, C. J.; Truhlar, D. G. Universal Solvation Model Based on Solute Electron Density and on a Continuum Model of the Solvent Defined by the Bulk Dielectric Constant and Atomic Surface Tensions. *J. Phys. Chem. B* **2009**, *113*, 6378−6396.
(63) Frisch, M. J.; Trucks, G. W.; Schlegel, H. B.; Scuseria, G. E.; Robb, M. A.; Cheeseman, J. R.; Scalmani, G.; Barone, V.; Petersson, G. A.; Nakatsuji, H.; Li, X.; Caricato, M.; Marenich, A. V.; Bloino, J.; Janesko, B. G.; Gomperts, R.; Mennucci, B.; Hratchian, H. P.; Ortiz, J. V.; Izmaylov, A. F.; Sonnenberg, J. L.; Williams-Young, D.; Ding, F.; Lipparini, F.; Egidi, F.; Goings, J.; Peng, B.; Petrone, A.; Henderson, T.; Ranasinghe, D.; Zakrzewski, V. G.; Gao, J.; Rega, N.; Zheng, G.; Liang, W.; Hada, M.; Ehara, M.; Toyota, K.; Fukuda, R.; Hasegawa, J.; Ishida, M.; Nakajima, T.; Honda, Y.; Kitao, O.; Nakai, H.; Vreven, T.; Throssell, K.; Montgomery, J. A., Jr.; Peralta, J. E.; Ogliaro, F.; Bearpark, M. J.; Heyd, J. J.; Brothers, E. N.; Kudin, K. N.; Staroverov, V. N.; Keith, T. A.; Kobayashi, R.; Normand, J.; Raghavachari, K.;

https://doi.org/10.1021/acs.iecr.2c01730
Ind. Eng. Chem. Res. 2022, 61, 9586−9599

Rendell, A. P.; Burant, J. C.; Iyengar, S. S.; Tomasi, J.; Cossi, M.; Millam, J. M.; Klene, M.; Adamo, C.; Cammi, R.; Ochterski, J. W.; Martin, R. L.; Morokuma, K.; Farkas, O.; Foresman, J. B.; Fox, D. J. *Gaussian 16*, revision B.01; Gaussian, Inc.: Wallingford, CT, 2016.
(64) Werner, H. J.; Adler, T. B.; Manby, F. R. Calculation of Small Molecular Interactions by Differences of Separate Total Energies−Some Procedures with Reduced Errors. *J. Chem. Phys* **2007**, *126*, No. 164102.
(65) Simon, S.; Duran, M.; Dannenberg, J. J. How Does Basis Set Superposition Error Change the Potential Surfaces for Hydrogen-Bonded Dimers? *J. Chem. Phys.* **1996**, *105*, 11024−11031.
(66) Villemin, D.; Moreau, B.; Elbilali, A.; Didi, M.-A.; Kaid, M.; Jaffrès, P.-A. Green Synthesis of Poly(Aminomethylenephosphonic) Acids. *Null* **2010**, *185*, 2511−2519.
(67) Jensen, M. K.; Kelland, M. A. A New Class of Hyperbranched Polymeric Scale Inhibitors. *J. Pet. Sci. Eng.* **2012**, *94*−*95*, 66−72.
(68) Mady, M. F.; Fevang, S.; Kelland, M. A. Study of Novel Aromatic Aminomethylenephosphonates as Oilfield Scale Inhibitors. *Energy Fuels* **2019**, *33*, 228−237.
(69) Mady, M. F.; Charoensumran, P.; Ajiro, H.; Kelland, M. A. Synthesis and Characterization of Modified Aliphatic Polycarbonates as Environmentally Friendly Oilfield Scale Inhibitors. *Energy Fuels* **2018**, *32*, 6746−6755.
(70) Mady, M. F.; Rehman, A.; Kelland, M. A. Synthesis and Antiscaling Evaluation of Novel Hydroxybisphosphonates for Oilfield Applications. *ACS Omega* **2021**, *6*, 6488−6497.
(71) Mady, M. F.; Bagi, A.; Kelland, M. A. Synthesis and Evaluation of New Bisphosphonates as Inhibitors for Oilfield Carbonate and Sulfate Scale Control. *Energy Fuels* **2016**, *30*, 9329−9338.
(72) Bromley, L. A.; Cottier, D.; Davey, R. J.; Dobbs, B.; Smith, S.; Heywood, B. R. Interactions at the Organic/Inorganic Interface: Molecular Design of Crystallization Inhibitors for Barite. *Langmuir* **1993**, *9*, 3594−3599.
(73) Yan, M.; Tan, Q.; Liu, Z.; Li, H.; Zheng, Y.; Zhang, L.; Liu, Z. Synthesis and Application of a Phosphorous-Free and Non-Nitrogen Polymer as an Environmentally Friendly Scale Inhibition and Dispersion Agent in Simulated Cooling Water Systems. *ACS Omega* **2020**, *5*, 15487−15494.
(74) Mady, M. F.; Abdel-Azeim, S.; Kelland, M. A. Investigation of the Antiscaling Performance of Phosphonated Chitosan for Upstream Petroleum Industry Application. *ACS Sustainable Chem. Eng.* **2021**, *9*, 16494−16505.
(75) Jones, F.; Piana, S.; Gale, J. D. Understanding the Kinetics of Barium Sulfate Precipitation from Water and Water−Methanol Solutions. *Cryst. Growth Des.* **2008**, *8*, 817−822.

https://doi.org/10.1021/acs.iecr.2c01730
Ind. Eng. Chem. Res. 2022, 61, 9586−9599